I&EC research
Industrial & Engineering Chemistry Research

pubs.acs.org/IECR

Article

Accurately Predicting CO_2 Reactive Absorption Properties in Aqueous Alkanolamine Solutions by Molecular Simulation Requiring No Solvent Experimental Data

Javad Noroozi* and William R. Smith*

Cite This: https://dx.doi.org/10.1021/acs.iecr.0c03738

Read Online

ACCESS | Metrics & More | Article Recommendations | Supporting Information

ABSTRACT: We present a general atomistic simulation framework for efficient reactive equilibrium calculations in dilute solutions, and its application to CO_2 reactive absorption in aqueous alkanolamine solutions. No experimental data of any kind are required for the solvents, and no empirical adjustments are required for its implementation. This hybrid methodology calculates reaction equilibrium constants by combining high-level quantum chemical calculations of ideal-gas standard reaction Gibbs energies (ΔG^0) with conventional solvation free energy calculations obtained from classical force field methodology. For these quantities we use explicit solvent molecular dynamics simulations with the General AMBER Force Field (GAFF). The resulting equilibrium constants are then coupled with a macroscopic Henry Law based ideal solution model to calculate the solution speciation and the CO_2 partial pressure, P_{CO_2}. We show results for seven primary amines: monoethanolamine (MEA), 2-amino-2-methylpropanol (AMP), 1-amino-2-propanol (1-AP), 2-amino-2-methyl-1,3-propanediol (AMPD), 2-aminopropane-1,3-diol (SAPD), 2-(2-aminoethoxy)ethanol or diglycolamine (2-AEE or DGA, respectively), and 2-amino-1-propanol (2-AP). Experimental speciation and P_{CO_2} data for some of these are available, with which we validate our methodology. We predict new results for others in cases when such data are unavailable, and provide explanations for the experimental inability to detect carbamate solution species in relevant cases. Our results for the pK value of the carbamate reversion reaction are within the chemical accuracy limit of $218.546/T$ units (corresponding to 1 kcal·mol^{-1} in the corresponding free energy change) in comparison with experimental results when such data exist, which at 298.15 K corresponds to 0.73 pK units. The precision of our pK predictions is comparable to that which can be obtained from conventional experimental methodologies for these quantities. Our results suggest that the presented molecular simulation methodology may provide a robust and cost-efficient tool for solvent screening in the design of post-combustion CO_2 capture processes.

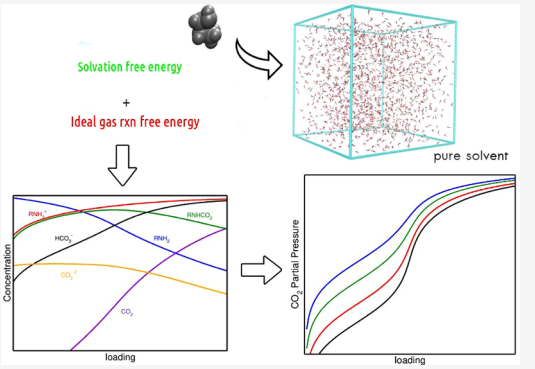

1. INTRODUCTION

Increasing atmospheric concentrations of CO_2 and other greenhouse gases and their consequent environmental effects have prompted a large body of research probing the CO_2 capturing properties of adsorbing materials and absorbing chemical solvents. Carbon capture and storage (CCS) is considered to be one of the most viable short-term options for reducing global carbon emissions.[1,2] Chemical absorption using aqueous alkanolamine solutions currently being used in industry are considered one of the most mature options for large-scale CO_2 capture.[3] However, the capture process suffers from several drawbacks, including high solvent regeneration energy costs, as a result of both parasitic energy losses, due to the high latent heat of the water cosolvent, and formation of the thermally stable carbamates, which also result in poor cyclic capacity.[4] In order to circumvent these problems, various alternative solvents, such as nonaqueous solvents,[5] lipophilic amines,[6] and phase changing compounds[7] have been recently considered. Unravelling the effects of different functional groups in the amine structures on their behavior is crucial for the design of improved alkanolamine-based CO_2 solvents. For example, heavily hindered alkanolamines have been shown to reversibly absorb CO_2 in an equimolar ratio and CO_2 can be completely desorbed at relatively low regeneration temperatures.[8]

The CO_2 capturing properties of the absorbent are a consequence of the kinetic and chemical reaction equilibrium properties resulting from the CO_2 dissolution, and the equilibrium composition of CO_2 in the solvent is an important tool for solvent screening. In the case of primary and secondary

Received: July 28, 2020
Revised: September 12, 2020
Accepted: September 14, 2020
Published: September 14, 2020

amines, CO_2 is absorbed primarily in the solution in the form of the carbamate ($RNHCO_2^-$), bicarbonate (HCO_3^-), and carbonate (CO_3^{-2}) species, in coexistence with the neutral (RNH_2) and protonated (RNH_3^+) amine species, water and its ionization products, and free CO_2.

The set of linearly independent chemical equations used to model chemical reaction equilibrium is governed only by the requirement that their number is $R = N - \text{rank}(\mathbf{A})$, where N is the number of species and $\mathbf{A}$ is the species formula matrix.[9] The actual set of reactions used need not be related to any postulated or actual reaction mechanics, and may be motivated by computational convenience. The following stoichiometry provides a convenient thermodynamic basis for describing the reaction equilibria of the indicated species in the case of primary and secondary amines.

$$2RNH_2 + CO_2 = RNH_3^+ + RNHCO_2^- \quad (R1)$$

$$RNHCO_2^- + H_2O = RNH_2 + HCO_3^- \quad (R2)$$

$$H_2O + CO_2 = HCO_3^- + H^+ \quad (R3)$$

$$HCO_3^- = CO_3^{-2} + H^+ \quad (R4)$$

$$H_2O = H^+ + OH^- \quad (R5)$$

$$CO_2(aq) = CO_2(vap) \quad (R6)$$

Tertiary amines do not form carbamates, and for these reactions R1 and R2 can be replaced by their sum

$$CO_2 + RNH_2 + H_2O = HCO_3^- + RNH_3^+ \quad (R7)$$

The equilibrium constants (or equivalently, the pK values) for reactions R3−R5 as functions of temperature are experimentally well-known. Their experimental determination for reactions R1 and R2 requires experimental data for each postulated solvent. Furthermore, the equilibrium constants can only be determined indirectly from such data, by fitting to the parameters of an empirically based chemical potential model.

pK values have been determined in this way by fitting to potentiometric titration measurements for the carbamate reversion reaction R2,[10] and for the amine protonation reaction,[10−16] which is the linear combination R1 + R2 − R3.

$$RNH_2 + H^+ = RNH_2^+ \quad (R8)$$

pK values have also been obtained by fitting thermodynamic models to experimental spectroscopically obtained speciation data of CO_2-loaded solutions.[17−21] In such experimental studies, the presence of the fast proton-exchanging species (*i.e*, the CO_3^{-2}/HCO_3^- or (RNH_3^+/RNH_2) pairs) complicates the data analysis, and usually only the total concentration of the carbonate/bicarbonate pair is available and can be used in the parameter fitting. Finally, parameters of chemical potential models and/or equations of state have been fitted to reaction models of CO_2 solubility data.[22] In other cases, the reactions have been approximated by pseudo-reaction physical association models incorporated in the SAFT[23−26] or the CPA[27,28] approaches.

Experimental screening of the vast number of potential solvent candidates is prohibitively expensive and time-consuming, and more predictive and less costly computational tools offer a promising alternative and complementary approach. The ability to accurately predict the equilibrium speciation and the associated CO_2 partial pressure for CO_2-loaded solutions of candidate solvents is one of the most important requirements, which is very challenging due to the complex chemical reaction and phase equilibria involved.

Three general approaches have been used toward this goal: combined Electronic Structure (ES) dielectric continuum solvent (DCS) models, *ab initio* Molecular dynamics (MD) methods, and classical force-field (CFF) methodologies. The first group includes methods based on the Conductor-like Screening Model for Realistic Solvents (COSMO-RS)[29,30] and Solvation Models based on Density (SMD).[31] These have been used to study reaction mechanisms and the relative stability of the carbamate product species.[32−35] Alternative DCS methods such as the SMDx family of Cramer et al.,[31] usually trained on hydration free energy data of neutral molecules at 298.15 K, may be potentially applied to such systems; however, their extension to ionic species and to higher temperatures has not been fully tested. Whereas the deficiencies of the continuum solvation models can be partially overcome by incorporating explicit solvent molecules in the first solvation shell,[36] their application to flexible molecules is not straightforward.[37]

In the second group, Nakai et al.[38−40] used density-functional tight-binding MD simulations to study reaction mechanisms in CO_2 chemical absorption and regeneration processes in aqueous amine solutions. While such approaches do not require *a priori* knowledge of the identities of the product species, they require detailed geometric criteria to dynamically evaluate their chemical identity and population at each step of the MD simulation. Moreover, such *ab initio* methods have only been carried out for relatively small system sizes and scale poorly with the system size, making them highly inefficient for the high throughput CO_2 solvent screening task. Other *ab initio* approaches based on first-principles calculations have also been developed and used for speciation predictions in reactive systems,[41] and they share the same disadvantages.

CFF methodologies have been employed by the groups of Vlugt et al.,[42] Maginn et al.,[43] and our group.[44,45] Balaji et al.[42] used the Reaction Ensemble (REMC) algorithm[46,47] (see also Johnson et al.[48]) in conjunction separately obtained ideal-gas electronic structure (ES) free energy calculations and fractional insertion of molecular species, in a preliminary study of reaction equilibria in the MEA−CO_2−H_2O system. Although the REMC algorithm was incorrectly implemented (by omitting the atomization energies in the ideal-gas ES calculations[44]), it was fortuitously able to reasonably predict the most abundant species (but not those present is minor concentrations) in the system at low to moderate CO_2 loadings. Mullen et al.[43] applied the REMC algorithm in conjunction with an enhanced Monte Carlo sampling approach for CO_2 absorption in a reactive ionic liquid. MC-based approaches for complex systems such as those involved in CO_2 reactive absorption generally suffer from the computational disadvantage in the case of even moderately complex molecules of requiring special system-specific sampling moves; they also require very long computation times and/or large system sizes to deal with the concentrations of species present in small amounts. These drawbacks make the REMC approach inefficient for their use in solvent screening.

Based on a recently developed reaction equilibrium algorithm requiring only straightforward conventional CFF-based MD free energy calculations, coupled with ES ideal-gas ES free energy calculations,[49] we recently implemented[44] a general and computationally efficient reaction equilibrium algorithm to predict speciation concentrations (including for species present

https://dx.doi.org/10.1021/acs.iecr.0c03738
Ind. Eng. Chem. Res. XXXX, XXX, XXX−XXX

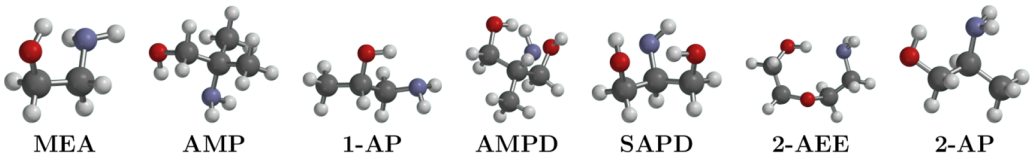

Figure 1. Molecular structures of the studied alkanolamines.

in very small concentrations) and P_{CO_2} in a preliminary study in the case of the benchmark CO_2−MEA−H_2O system.

The goal of this paper is to improve this CFF-based methodology and to illustrate its application to the accurate prediction of CO_2 reactive absorption speciation and P_{CO_2} data as functions of loading, temperature, and solvent composition, for aqueous MEA and for six additional primary alkanolamine systems, whose molecular structures are shown in Figure 1. Where experimental data are available, we compare our predictions with experimentally obtained P_{CO_2} and solution speciation data in the literature. For situations in which experimental data are unavailable, our calculations provide predictions that await experimental verification.

2. MOLECULAR-BASED THERMODYNAMIC METHODOLOGY

A major challenge in implementing reaction equilibrium calculations from molecular simulations is the expression of the macroscopic thermodynamic models involved in terms of molecular simulation quantities. These little known relationships are briefly described in this section.

The equilibrium composition of a closed chemically reacting system at specified (T, P) can be obtained by minimizing its Gibbs free energy subject to the conservation of mass and electroneutrality constraints, and implemented by calculating the solution of the R equations

$$\Delta G_j(T, P; \mathbf{x}) \equiv \sum_{i=1}^{N_s} \nu_{ij}\mu_i(T, P; \mathbf{x}) = 0; \quad j = 1, 2, ..., R \tag{1}$$

where ν_{ij} is the stoichiometric coefficient of species i in reaction j and $\mathbf{x}$ represents the system composition vector. The reaction equilibrium composition can be readily accomplished by a wide range of numerical algorithms[9] and chemical potential models, and we employ here a Henry Law based model. The chemical potentials (for both solutes and solvent) in this model are expressed as

$$\mu_i(T, P; \mathbf{m}) = \mu_i^{\dagger}(T; P) + RT \ln\left(\frac{m_i}{m^0}\right) + RT \ln \gamma_i(T, P; \mathbf{m}); \quad i = 1, 2, ..., N_{solu} \tag{2}$$

where T is the absolute temperature, P is the pressure, R is the universal gas constant, m_i is the molality of species i, γ_i is its Henry Law activity coefficient, and $\mathbf{m}$ is the vector of species molalities. $m^0 = 1$ mol·kg^{-1} solvent.

We have previously shown[50] that the standard chemical potential $\mu_i^{\dagger}(T; P)$ of solute species i can be calculated in terms of molecular simulation quantities by

$$\mu_i^{\dagger}(T, P) = \mu_i^{0}(T; P^0) + RT \ln\left(\frac{RTM_{solv}m^0\rho^*_{solv}(T, P)}{1000P^0}\right) + \mu_i^{res,NVT;\infty}[T, \rho^*_{solv}(T, P)] \tag{3}$$

where $P^0 = 1$ bar is the standard state pressure and $\mu_i^{0}(T; P^0)$ is the ideal gas chemical potential of species i, which can be calculated from the partition function of its ideal-gas molecule under the harmonic oscillator rigid rotor approximation,[51,52] $\rho^*_{solv}(T, P)$ is the density of the pure solvent (water in our case), M_{solv} is its molecular weight, and $m^0 = 1$ mol·kg^{-1} solvent. For a solute, $\mu_i^{res,NVT;\infty}[T, \rho^*_{solv}(T, P)]$ is its residual chemical potential at infinite dilution in the solvent (also referred to as its intrinsic hydration free energy, $\Delta G_{hyd}(T, P)$), and the same quantity for the solvent is its self-solvation free energy; both are calculated by conventional MD simulations in the NVT ensemble.

In the following, we restrict attention to the ideal solution approximation, $\gamma_i = 1$ (expressions for the nonideal case are given in our previous paper[44]). The solvent chemical potential is obtained from the Gibbs−Duhem equation as[44]

$$\mu_{solv}(T, P; \mathbf{m}) = \mu^{\dagger}_{solv}(T; P) + RT \ln\left(\frac{1000}{M_{solv}m^0}\right) - RT\left(\frac{1 - x_{solv}}{x_{solv}}\right) \tag{4}$$

We remark that, for reactions in which the solvent (here water) participates, the solvent chemical potential is typically approximated in experimental studies by its Raoult Law form

$$\mu_{solv}(T, P; \mathbf{m}) = \mu^*_{solv}(T, P) + RT \ln(x_{solv}) \tag{5}$$

where $\mu^*_{solv}(T, P)$ is the pure solvent chemical potential and x_{solv} is its mole fraction. Substitution of eqs 2−4 in eq 1 yields the final working equations:

$$\frac{\Delta\tilde{G}_j(T, P)}{RT} + \sum_{i=1}^{N_{solu}} \nu_{ij} \ln\left(\frac{m_i}{m^0}\right) + \nu_{solv,j}\left(\frac{x_{solv} - 1}{x_{solv}}\right) = 0; \quad j = 1, 2, ..., R \tag{6}$$

where $\nu_{solv,j}$ is the stoichiometric coefficient of the solvent in reaction j, and

$$\Delta\tilde{G}_j(T, P) = \Delta G_j^0(T; P^0) + \Delta G_j^{res,NVT;\infty}(T, P) \tag{7}$$

$$+RT\overline{\nu}_j \ln\left(\frac{RTM_{solv}m^0\rho^*_{solv}(T, P)}{1000P^0}\right) + \nu_{solv,j}RT \ln\left(\frac{1000}{M_{solv}m^0}\right) \tag{8}$$

where

https://dx.doi.org/10.1021/acs.iecr.0c03738
Ind. Eng. Chem. Res. XXXX, XXX, XXX−XXX

$$\Delta G_j^0(T;\ P^0) = \sum_{i=1}^{N_s} \nu_{ij}\ \mu_i^{\ 0}(T;\ P^0) \tag{9}$$

$$\Delta G_j^{\mathrm{res},NVT;\infty}(T,\ P) = \sum_{i=1}^{N_s} \nu_{ij}\ \mu_i^{\mathrm{res},NVT;\infty}(T;\ P) \tag{10}$$

$$\overline{\nu_j} = \sum_{i=1}^{N_s} \nu_{ij} \tag{11}$$

$\Delta\tilde{G}_j(T,\ P)$ is commonly expressed in terms of the equilibrium constant K_j, via

$$\mathrm{p}K_j(T,\ P) \equiv -\log_{10} K_j = \frac{\Delta\tilde{G}_j(T,\ P)}{RT\ \ln(10)} \tag{12}$$

We remark that the third term in eq 8 can be separated into a temperature-dependent term (often referred to as the "standard state correction") and a density term, which is often mistakenly neglected in pK calculations (see Noroozi and Smith[45]).

3. SIMULATION DETAILS

3.1. Ideal-Gas Reaction Free Energies. In order to find the most stable conformer of the molecular/ionic species, an extensive gas phase conformational search was first performed for the geometries of the protonated, carbamate, and neutral forms of each amine using the Merck Molecular Mechanics Force Field (MMFF94) implemented in the Spartan v.18 Software package.[53] For each species, for each of the 10 lowest energy conformers obtained from this search we performed further geometry optimizations to find the lowest free energy conformers arising from five different high-level composite quantum chemical (QM) methods: G4, G3, G3B3, CBS-QB3, and CBS-APNO in Gaussian16.[54] We ensured that, for each QM method, the conformer converged to a stable minimum of the potential energy surface with positive real vibrational frequencies. We then used the conformer with the lowest free energy/chemical potential for the subsequent ideal-gas reaction free energy calculations for each of the five QM methods. The combination of the results of these five methods is described in the Results and Discussion section.

3.2. Force Field Development and Hydration Free Energy Calculations. For the amine's neutral (RNH_2), protonated (RNH_3^+), and carbamate ($RNHCO_2^-$) forms, and for the bicarbonate ion (HCO_3^-), the Lennard–Jones (LJ) and intramolecular bonded (bond stretching, angle bending, and dihedral torsion) potential parameters of the force fields were modeled in a consistent manner using the General Amber Force Field[55] parameters within its default functional form by using the Antechamber package in AMBER tools,[56] which employs an algorithm to assign the parameters based on the atom types. Carbon dioxide (CO_2) was modeled using the TraPPE potential of Pottof,[57] and to be consistent with GAFF parametrization the solvent (water) was modeled with the TIP3P Force Field.

To calculate the partial charges, high-level QM methods are generally preferred to refine the geometry of the lowest-energy solute conformer as described in the previous section. However, to be consistent with the ideal-gas geometry of the force fields in the hydration free energy calculations, we used the lowest free energy conformer at the G4 level of the previous section as representative of the solute gas-phase geometry to calculate its electrostatic potential energy grid at the GAFF default HF/6-31G* level using the Merz–Kollman scheme in Gaussian16. We also examined the effects of determining the partial charges from several different QM electron density determination methodologies (B3LYP/6-311++G(d,p), MP2/aug-cc pVTZ, and MP2/aug-cc pVTZ+PCM) on the resulting hydration free energies and the equilibrium constants, which is discussed in Section 4.3.

Finally, we used the two-step Restrained Electrostatic Surface Potential (RESP) fitting method[58] within the Antechamber software package to assign the partial charges. The Gromacs-formatted topologies were then generated using the acpype (version 2019) python interface.[59]

MD simulations of the hydration free energies in eq 11 were performed using a single solute molecule solvated in a periodic box of 1500 water molecules using the Gromacs (version 2016.3) program,[60] with initial configurations generated using the packmol software package.[61] A steepest-descent minimization was then performed to remove any bad contacts, followed by a short (100 ps) NVT equilibration run followed by a 12 ns NPT simulation with the first 2 ns discarded to determine the system density. Free energy simulations to decouple the solute molecule from its solvent environment were then initiated from the equilibrated configurations in an NVT ensemble, with the box size corresponding to the calculated density.

The equations of motion were integrated using the Gromacs stochastic Langevin scheme, with a friction constant of 1.0 ps^{-1}. The pressure was maintained using a Parrinello–Rahman pressure coupling constant of 2.0 ps. The Lennard–Jones short-range interactions were smoothly switched off between 12 and 12.5 Å, and the electrostatic interactions were computed using the particle mesh Ewald (PME) method with a 12 Å real-space cutoff, 1.0 Å grid spacing, sixth-order spline interpolation, and accuracy of 10^{-6}. The free energy of decoupling the solute molecule from its solvent environment was calculated using the Gromacs Bennett Acceptance Ratio (BAR) method (gmx bar). We employed six equally spaced λ values and linear decoupling for the electrostatic interaction, followed by 20 equally spaced λ values with $\Delta\lambda = 0.05$ to decouple the LJ interactions using the standard GROMACS soft-core potential function originally proposed by Beutler et al.,[62] with parameters (in GROMACS notation) *sc-alpha* = 0.5, *sc-power* = 1 and *sc-sigma* = 0.3. For each alchemical window, we used a 12.5 ns simulation with the first 2.5 ns discarded for equilibration.

4. RESULTS AND DISCUSSION

4.1. Ideal–Gas Standard Reaction Free Energies. Tables S1 and S2 of the Supporting Information show our calculated ideal-gas standard reaction free energies $\Delta G_j^0(T;\ P^0)$ of eq 9 for reactions R1 and R2 at the four temperatures (298.15 K, 313.15 K, 333.15 K, 353.15 K) for the set of seven amines considered, using five different composite QM methods.

As noted by Somer et al.,[63] improved predictions can arise from the use of combinations of several high level methods, since methods such as G4 tend to overestimate and methods such as CBS-QB3 tend to underestimate the reaction free energy. The variations in the different methods also enable us to infer the uncertainty rooted in the different chemical species of the same class of molecules. For example, in our previous work,[45] we found that for the amine species, the ideal gas free energies vary significantly among the QM methods, depending on the size and flexibility of the molecules involved. Based on the Table S1 results, for most species the Gaussian-n theories (G4, G3,

https://dx.doi.org/10.1021/acs.iecr.0c03738
Ind. Eng. Chem. Res. XXXX, XXX, XXX−XXX

Table 1. Predicted pK Values for reactions R1 and R2 from This Work at the Indicated Temperatures and P = 1 bar

T (K)	MEA	AMP	1-AP	AMPD	SAPD	2-AEE	2-AP
				Reaction R1			
298.15	$-5.75_{0.56}$	$-2.29_{0.58}$	$-3.89_{0.66}$	$-2.24_{0.52}$	$-3.63_{0.62}$	$-5.84_{0.50}$	$-3.57_{0.49}$
313.15	$-4.84_{0.54}$	$-1.58_{0.55}$	$-3.08_{0.63}$	$-1.69_{0.51}$	$-2.95_{0.59}$	$-4.93_{0.49}$	$-2.88_{0.46}$
333.15	$-3.83_{0.49}$	$-0.74_{0.52}$	$-2.30_{0.60}$	$-0.80_{0.50}$	$-2.11_{0.55}$	$-3.77_{0.48}$	$-2.05_{0.44}$
353.15	$-3.20_{0.50}$	$-0.01_{0.49}$	$-1.61_{0.58}$	$-0.32_{0.49}$	$-2.05_{0.51}$	$-2.63_{0.48}$	$-1.37_{0.41}$
				Reaction R2			
298.15	$1.62_{0.42}$	$-1.87_{0.50}$	$0.61_{0.40}$	$-1.02_{0.60}$	$-0.095_{0.53}$	$1.22_{0.66}$	$-0.26_{0.48}$
313.15	$1.38_{0.40}$	$-1.93_{0.49}$	$0.43_{0.39}$	$-1.08_{0.59}$	$-0.19_{0.51}$	$0.90_{0.65}$	$-0.34_{0.47}$
333.15	$1.15_{0.39}$	$-1.90_{0.47}$	$0.30_{0.37}$	$-1.16_{0.57}$	$-0.28_{0.49}$	$0.59_{0.63}$	$-0.42_{0.45}$
353.15	$1.15_{0.38}$	$-1.90_{0.46}$	$0.25_{0.36}$	$-1.14_{0.55}$	$-0.38_{0.48}$	$0.18_{0.62}$	$-0.47_{0.44}$

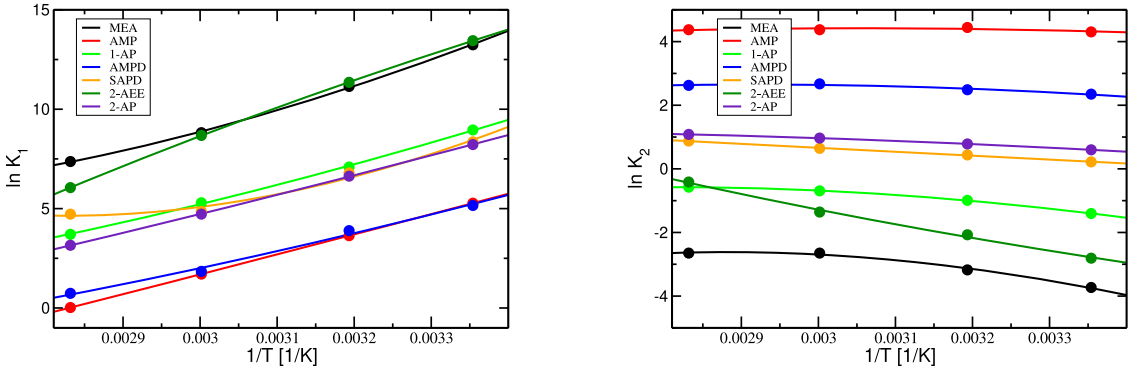

Figure 2. Temperature dependence of the equilibrium constants for reactions R1 and R2 for the seven amines studied.

G3B3) tend to predict higher $\Delta G_j^0(T; P^0)$ values than those of the complete basis set (CBS-QB3, CBS-APNO) approaches. We note that the R2 values generally indicate slightly smaller standard deviations than those of R1, except for the species containing multiple hydroxyl groups (SAPD, AMPD, 2-AEE). For these species reaction R2 shows significant scatter among the QM methods.

For speciation calculations involving reactions R1 and R2, we used the average $\Delta G_j^0(T; P^0)$ values from the five methods in Tables S1 and S2. Tables S8−S12 show the raw Gaussian16[60] output for each species from which they were calculated. Their standard deviations are about 3 kJ·mol^{-1}, which we take as a surrogate measure of the uncertainty in the $\Delta G_j^0(T; P^0)$ values. This value is well within a "chemical precision standard" of 1 kcal·mol^{-1}.

4.2. Equilibrium Constants pK_1 and pK_2. Table 1 summarizes our pK_1 and pK_2 results for the seven alkanolamines studied at the indicated temperatures and P = 1 bar. The underlying data used for their calculation are given in the Supporting Information as follows. Table S4 shows the simulated $\mu^{res,NVT;\infty}(T, P)$ values for the neutral (RNH_2), protonated (RNH_3^+), and carbamate ($RNHCO_2^-$) forms of the seven alkanolamines at the four temperatures of this study. Table S5 shows $\mu^{res,NVT;\infty}(T, P)$ values for HCO_3^-, for CO_2 using the Trappe FF,[57] and for H_2O using the TIP3P FF. The $\Delta\tilde{G}_j(T, P)$ and p$K_j(T, P)$ values for reactions R1 and R2 used in the reaction equilibrium calculations listed in Tables S6 and S7.

The indicated uncertainties are one standard deviation, which are seen to be within a "chemical precision standard" of 1 kcal·mol^{-1} for $\Delta\tilde{G}_j(T, P)$ in eq 8. This translates to a precision in pK units of

$$\Delta \mathrm{p}K = \frac{4184}{2.303RT} = \frac{218.546}{T} \tag{13}$$

which at 298.15 K is 0.73 pK units.

The dependence of the equilibrium constants on temperature is shown in Figure 2, using regressions to the expression

$$\mathrm{p}K = a + b/T + c\ln(T) \tag{14}$$

The values of the parameters (a, b, c) are given in Table S3 of the SI. Interestingly, the right panel of Figure 2 shows that, in comparison with the carbamate forming amines (MEA, 1-AP, 2-AEE), the pK_2 values for the sterically hindered amines (AMP, AMPD, SAPD, 2-AP) show a weaker temperature dependence.

4.3. Effects of Different Partial Charge Methods on the pK Values. As described in Section 3, for the pK calculations and the resulting equilibrium compositions we used the default HF/6-31G* partial charges based on each molecule's G4 optimized geometry, from which the electrostatic surface grid and the RESP atomic partial charges were obtained. Numerous studies[64,65] have addressed the effects on the $\mu^{res,NVT;\infty}$ values of different QM approaches used to obtain the FF partial charges. To examine this effect for our systems, we considered representative $\mu^{res,NVT;\infty}$ values for MEA and for AMP at T = 298.15 K based on RESP partial charge assignment arising from several different QM methodologies: the default GAFF HF/6-31G* results from Table S3, B3LYP/6-311++G(d,p), MP2/aug-cc-pVTZ) in the gas phase, and a MP2/aug-cc-pVTZ calculation in the presence of polarizable continuum solvent (MP2/aug-cc-pVTZ+PCM, with a dielectric constant of 78.39). These are shown in Table 2.

https://dx.doi.org/10.1021/acs.iecr.0c03738
Ind. Eng. Chem. Res. XXXX, XXX, XXX−XXX

Table 2. Comparison of GAFF Predicted Intrinsic Hydration Free Energies, $\mu^{res,NVT;\infty}$ (in kJ·mol^{-1}) of the Protonated, Neutral, And Carbamate Forms of MEA and AMP at T = 298.15 K Using Different Sets of Partial Charges in Conjunction with RESP

Species	MP2/aug-cc-pVTZ+PCM	HF/6-31G*	B3LYP/6-311++G(d,p)	MP2/aug-cc-pVTZ
		monoethanolamine (MEA)		
RNH_2	$-32.89_{0.05}$	$-30.23_{0.14}$	$-26.94_{0.19}$	$-23.30_{0.07}$
RNH_3^+	$-243.87_{0.09}$	$-239.43_{0.10}$	$-235.95_{0.1}$	$-234.71_{0.13}$
$RNHCOO^-$	$-400.63_{0.08}$	$-366.79_{0.19}$	$-365.63_{0.15}$	$-358.62_{0.27}$
		2-amino-2-methylpropanol (AMP)		
RNH_2	$-38.53_{0.03}$	$-34.35_{0.13}$	$-31.68_{0.16}$	$-27.50_{0.07}$
RNH_3^+	$-228.33_{0.06}$	$-222.50_{0.11}$	$-216.22_{0.13}$	$-215.57_{0.12}$
$RNHCOO^-$	$-393.84_{0.06}$	$-352.33_{0.10}$	$-349.64_{0.12}$	$-342.94_{0.04}$

The results show relatively small (3−8 kJ·mol^{-1}) differences from our default HF/6-31G* calculations in the cases of B3LYP/6-311++G(d,p) and MP2/aug-cc-pVTZ). However, when the polarizable continuum model (PCM) is included in the calculation of the electron density (MP2-aug-cc-pVTZ +PCM), the hydration free energy of the carbamate anion ($RNHCO_2^-$) becomes considerably more negative (by 30−40 kJ·mol^{-1}) compared to the unpolarized charge density (mp2-aug-cc-pVTZ) result. In contrast, the charges derived from the polarized electronic density causes the hydration free energy of the protonated amines (RNH_3^+) becomes more negative by only 5−6 kJ·mol^{-1}. Partial charges obtained from the RESP methodology already tend to over polarize anions in the absence of PCM,[66] and our results show that this becomes excessive in its presence.

Representative pK values at 298.15 K for reactions R1 and R2 calculated from eqs 8−12 using columns 3−5 of Table 2 and the data of Tables S1, S2, and S4 are shown in Table 3. Whereas the

Table 3. Comparison of the Predicted pK Values of Reactions R1 and R2 for the MEA and AMP Systems at T = 298.15 K Using Different Sets of Partial Charges from Table 2, the ΔG^0 Values in Table S1 and S2, and the $\mu^{res,NVT;\infty}$ Values for H_2O, CO_2, and HCO_3^- in Table S4

Reaction	HF/6-31G*	B3LYP/6-311++G(d,p)	MP2/aug-cc-pVTZ
		monoethanolamine (MEA)	
R1	$-5.75_{0.56}$	$-6.09_{0.56}$	$-5.92_{0.56}$
R2	$1.62_{0.42}$	$2.00_{0.41}$	$1.41_{0.41}$
		2-amino-2-methylpropanol (AMP)	
R1	$-2.29_{0.58}$	$-1.64_{0.58}$	$-1.81_{0.58}$
R2	$-1.87_{0.50}$	$-1.85_{0.50}$	$-1.31_{0.50}$

$\mu^{res,NVT;\infty}$ vary substantially across the QM levels in Table 2, the pK values in Table 3 are not overly sensitive to the different partial charge methodologies. However, we note that our comparisons were obtained using GAFF Lennard−Jones force-field parameters, which are optimized to the HF/6-31G* partial charges. A more complete comparison of the effects of the different theories/levels on the hydration free energies would require re-optimization with respect to experiment of the Lennard−Jones force-field parameters for each theory/level. Since the partial charges tend to be the major contribution to the hydration free energy values, we do not expect such a reoptimization to produce a large effect. In any event, such a study is beyond the scope of this work, and would also contradict its purely predictive approach.

4.4. Carbamate Stability Constant, K_2. In this section we discuss our results for the equilibrium constant K_2 of the carbamate reversion reaction R2 (the inverse of the carbamate formation reaction equilibrium constant), in comparison with those obtained from experiment at the representative temperature 298.15 K when such data are available.

In our approach, we directly predict $K_2(T, P)$ from simulation quantities using eq 12. $K_2(T, P)$ cannot be directly measured experimentally, but must be obtained indirectly using

$$\ln K_2(T, P) = \sum_{i=1}^{N_s} \nu_{i2}[\ln m_i^* + \ln \gamma_i(T, P; \mathbf{m}^*)] \quad (15)$$

where the molalities and activity coefficients refer to an experimentally measured equilibrium composition, $\mathbf{m}^*$, and ν_{i2} is the reaction stoichiometric coefficient of species i in reaction R2. One approach is by means of extrapolation to zero ionic strength of the experimentally measured species activity coefficients of eq 15, and another is by fitting the measured equilibrium data to the parameters of a thermodynamic model for the chemical potentials.

Our predicted pK_2 values at the representative temperature T = 298.15 K are shown in Table 4, where they are compared with experimental results from the literature. The major source of uncertainty in our pK calculations is that of the ideal-gas ΔG_2^0 term in eq 9. For the experimental values, the sources of uncertainty/error in pK_2 are the uncertainties in any model used

Table 4. Comparison with Literature Data of Calculated pK_2 for the Carbamate Reversion Reaction R2 at T = 298.15 K (unless Indicated Otherwise) and P = 1 bar

Amine	This work, Table 2	Literature
monoethanolamine (MEA)	$1.62_{0.42}$	1.71(291.15 K),[67] 1.25,[68] 1.31,[69] 1.86[70] 1.81,[71] 1.46,[72] 1.60,[73] $1.76_{0.02}$[18]
2-amino-2-methyl-1-propanol (AMP)	$-1.87_{0.50}$	−2.15,[a] −1.66,[74] <−0.70(303 K),[17] <−1,[75] −1.0[76]
1-amino-2-propanol (1-AP)	$0.61_{0.40}$	$1.70_{0.2}$[77]
2-amino-2-methyl-1,3-propanediol (AMPD)	$-1.02_{0.60}$	sterically hindered
2-(2-aminoethoxy) ethanol (2-AEE)	$1.22_{0.66}$	1.75[78]
serinol(2-aminopropane-1,3-diol) (SAPD)	$-0.09_{0.53}$	no carbamate detected[77]
2-amino-1-propanol (2-AP)	$-0.26_{0.48}$	$0.6_{0.1}$,[77] 0.98[18]

[a]Calculated from the mole-fraction-based apparent equilibrium constant of 0.47 from Ciftja et al.[79]

https://dx.doi.org/10.1021/acs.iecr.0c03738
Ind. Eng. Chem. Res. XXXX, XXX, XXX−XXX

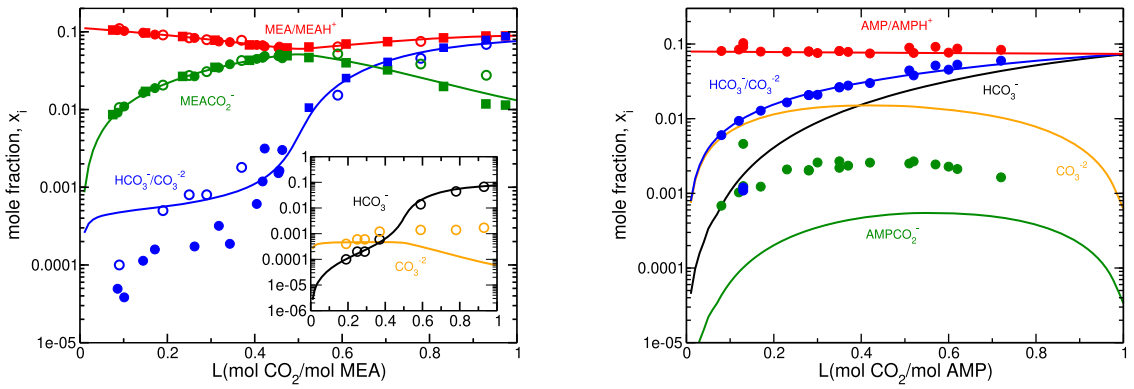

Figure 3. Speciation predictions (curves) for 30 wt % aqueous MEA and AMP solutions of CO_2 at T = 298.15 K and P = 1 bar, and their comparison with experimental data. For MEA/$MEAH^+$, all experimental data points are indistinguishable and fall on the predicted curve. For MEA carbamate, open green circles are data of Jakobsen et al.,[90] filled green circles are data of Hilliard[91] and filled green squares are data of Böttinger et al.[71]). For the MEA HCO_3^-/CO_2^{-2} data, open blue data points refer to the separately measured and subsequently combined data of Jakobsen et al.[90] (the separate concentrations are shown in the inset); filled data points refer to measurements of the combination only (filled blue circles of Hilliard[91] and filled blue squares of Böttinger et al.[71] The data of Jakobsen et al.[90] and of Böttinger et al.[71] are at 293.15 K, and the data of Hilliard are at 300.15 K. Experimental data for AMP are from Ciftja et al.[74] at 298.15 K.

for the activity coefficients and the uncertainties in the experimental composition measurements. The latter is likely the greater contributor, since both the neutral and the protonated amine pair are present as is the case for the bicarbonate/carbonate pair, and it is very difficult to experimentally distinguish the individual species concentrations from NMR data.

We have already noted that our pK uncertainties are within a "chemical precision standard" of 0.73 pK units at 298.15 K. We remark that the precisions of experimental studies are often not provided in their publications (but we highlight the careful experimental work of the Tremaine group,[20] which recently studied pK_2 values from 283.2−313.2 K for 2-methylpiperadine using NMR spectroscopy and reported precisions of 0.35−1.50 pK units).

p$K_2(T, P)$ for MEA has been the subject of numerous experimental studies,[17,18,69,73,77] using the indicated approaches or variants thereof. For MEA at 298.15 K, our predictive methodology gives pK_2 = 1.62 ± 0.42. The spread of the literature pK values (1.25−1.86) is partly due to differences in the activity coefficient models used by the authors and, likely more importantly, to the difficulty in the measurement of the concentrations of the proton exchanging species. The precision of our prediction is seen to be similar to that of the experimentally measured values. (See also Section 6.)

There are fewer experimental pK_2 results for the other alkanolamines. Several groups[20,74−76,78,79] have reported an "apparent equilibrium constant" for pK_2 for a range of solvents based on the approximations that the activity of water is unity and that the activity coefficients for $RNHCO_2^-$ and HCO_3^- are equal and hence cancel in the activity coefficient ratio at all concentrations. The latter behavior (referred to herein as the iso-Colombic approximation, ICA) is based on the fact that the cancellation holds exactly in the Debye−Hückel activity coefficient model for the iso-Coulombic reaction R2 at all concentrations. pK_2 obtained from the ICA is referred to as an "apparent equilibrium constant". We can see mild supporting evidence for the ICA from the $\mu^{res,NVT;\infty}$ values for $RNHCO_2^-$ and HCO_3^- in Tables S3 and S4 of the Supporting Information, where it is seen that they are of the same sign and similar magnitude. We also found (not shown) that simulations show that this behavior continues to hold as the solution concentrations increase.

Our predicted AMP value is pK_2 = −1.87 ± − 0.50. McCann et al.[17] studied the AMP system using ^{1}H NMR. They did not detect carbamate, but they noted that pK_2 < −0.70 at 303 K. Other authors reported apparent equilibrium constants based on the ICA. Sartorl and Savage[75] reported pK_2 < −1.0 at 313 K in their ^{13}C NMR study. Ciftja et al.[79] obtained a value of pK_2 = −2.15 and later[74] a value of pK_2 = −1.66, based on ^{13}C NMR measurements. Yamada et al.[76] reported pK_2 ≈ −1.0 for AMP from ^{13}C NMR studies. The negative AMP pK_2 value compared to that of MEA indicates that AMP carbamate formation is thermodynamically less favored, a consequence of the steric effect of the two methyl groups ($-CH_3$) on the α carbon connected to the amine nitrogen atom.

The addition of a $-CH_3$ group to the β carbon of MEA gives 1-AP. For this molecule, we predict a carbamate formation constant of pK_2 = 0.61 ± 0.40, which is smaller than that of MEA. This indicates a small steric effect, arising from the $-CH_3$ group being further away from the amino group. The experimental study of Conway et al.[77] also noted significant carbamate formation in the 1-AP solution, and they reported pK_2 = 1.7.

We did not find any experimental carbamate/bicarbonate concentration data for AMPD. Similarly to AMP, it is a sterically hindered amine and we predict pK_2 = −1.02 ± 0.60.

For 2-AEE, we predict pK_2 = 1.21 ± 0.66 at 298.15 K; this system was experimentally studied by Al-Juaied et al.[78] using ^{13}C NMR, who reported an apparent pK_2 = 1.75 for 17.7 M 2-AEE at relatively low CO_2 loading at 300 K. (See the iso-Coulombic discussion above.)

While Conway et al.[77] did not observe carbamate formation in SAPD, Bougie et al.[80] suggested carbamate formation in SAPD similar to that of unhindered amines based on the trend of the solubility data. For SAPD, we predict a value of pK_2 = −0.09 ± 0.53 at 298.15 K, indicating that it is a mildly carbamate-forming amine.

Removing one of the $-CH_3$ groups from the α carbon of AMP gives 2-AP. For 2-AP, the predicted pK_2 value increases to pK_2 = −0.26 ± −0.48, which lies between that of MEA and AMP. Fernandes et al.[18] reported a value of pK_2 = 0.98 at 298.15 K for

https://dx.doi.org/10.1021/acs.iecr.0c03738
Ind. Eng. Chem. Res. XXXX, XXX, XXX−XXX

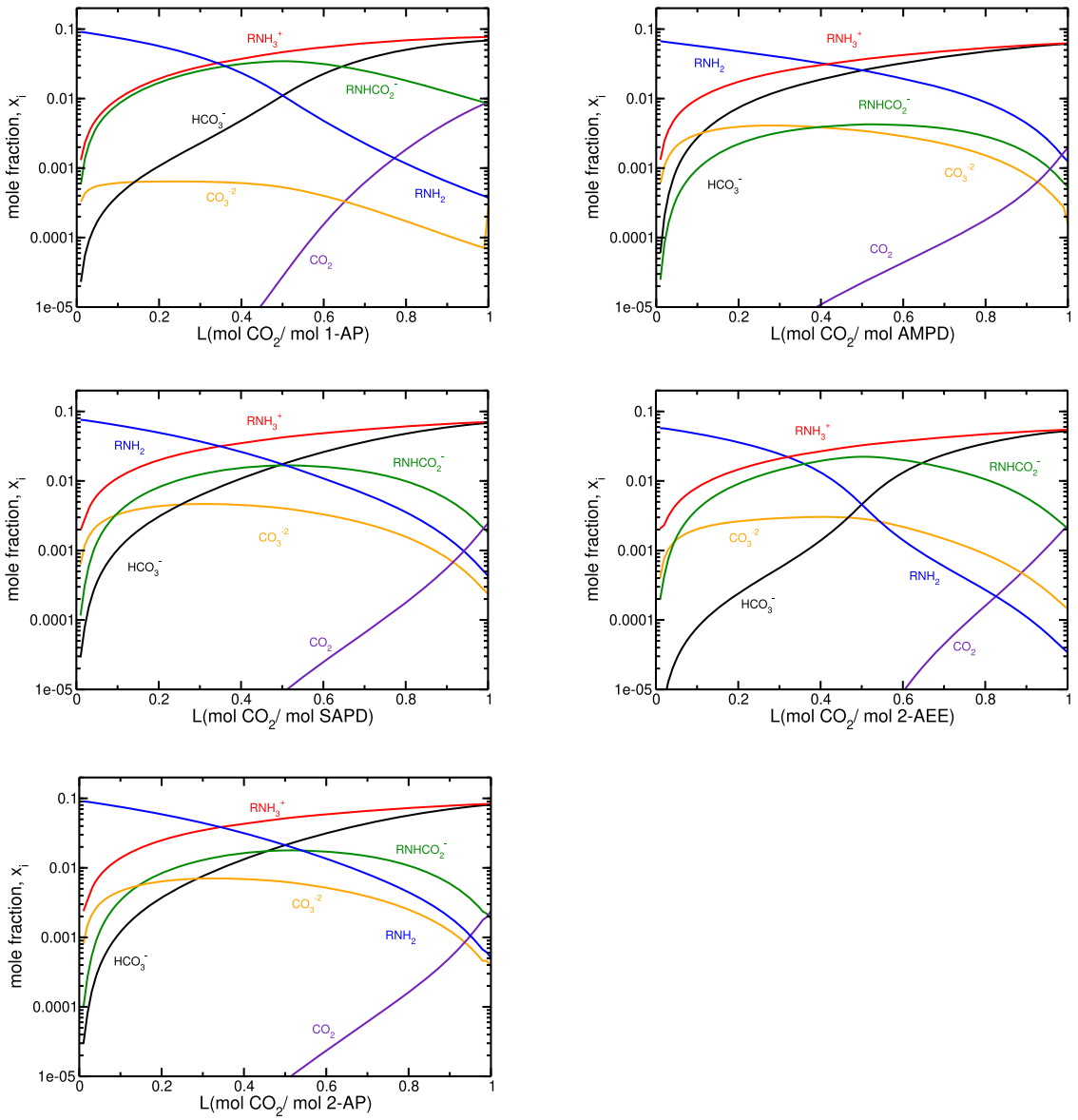

Figure 4. Speciation predictions (curves) for reactive absorption of CO_2 in 30 wt % amine aqueous solutions at T = 298.15 K and P = 1 bar. No experimental data exists for comparison.

2-AP from their NMR study. In a more recent study by the same group,[77] they obtained pK_2 = 0.6 ± 0.1, which agrees with our predicted value within their mutual uncertainties.

Figures 3 and 4 of Section 4.6 show the decreasing carbamate concentrations for the solvents as their pK_2 value decreases. For AMP, the alkanolamine with the lowest pK_2 value, evidence of the experimental difficulty of observing carbamate is indicated in Figure 3, where it is seen that its carbamate mole fraction becomes less than 10^{-4} at low and at high CO_2 loadings.

In general, comparison with the (often limited) experimental data shows that the molecular models employed here are able to capture, qualitatively and to a reasonable quantitative accuracy, the observed trend in the steric effects on carbamate formation for the common primary amines used in the PCC process studied herein.

4.5. Consistency Tests for the Amine Protonation Constants. For a wide range of amines, experimental data are available for the amine protonation reaction pK_8 of reaction R8.[89] Furthermore, the equilibrium constants for reactions R3−R5 are well studied, based on the CO_2−H_2O equilibria for a wide range of temperatures.[81] Since reaction R8 is the sum R1 + R2 − R3, this allows the prediction of any one of the equilibrium constants from those of the others. In particular, this approach allows the prediction of amine protonation pK_8 values from molecular simulation that are independent of knowledge of the intrinsic hydration free energy of the proton, precise values of which remain unknown despite extensive experimental and theoretical efforts.

In Table 5, we show predictions of pK_8 from our simulation results for the equilibrium constants of reactions R1 and R2 in conjunction with the experimental data of Edwards et al.[81] for the bicarbonate reaction R3. It is seen that the pK_8 values predicted in this way are generally within 1 pK unit of the experimental values. Since we have previously seen that our pK_2 values agree well with the corresponding experimental values and the only species not appearing in both R1 and R2 is the protonated amine species, RNH_3^+, we conjecture that an

https://dx.doi.org/10.1021/acs.iecr.0c03738
Ind. Eng. Chem. Res. XXXX, XXX, XXX−XXX

Table 5. Prediction of the Amine Protonation Constant pK_8 Independently of Knowledge of the Proton (H^+) Hydration Free Energy at 298.15 K Using $pK_8 = pK_1 + pK_2 - pK_3$, in Conjunction with Our Results for pK_1 and pK_2 in Table 1 and the Well-Established Experimental Value $pK_3 = 6.30$[81] for the Bicarbonate Reaction R3

amine	$-pK_8$ (this work)	$-pK_8$ (expt)
MEA	$10.42_{0.50}$	9.51,[82] 9.44,[83] 9.50,[84] $9.51_{0.01}$[85] $9.59_{0.19}$,[86] 9.50,[87] $9.44_{0.01}$[88]
AMP	$10.45_{0.52}$	$9.67_{0.01}$[18]
1-AP	$9.57_{0.56}$	9.50
AMPD	$9.63_{0.44}$	$8.84_{0.01}$[18]
SAPD	$10.07_{0.55}$	8.55
2-AEE	$10.97_{0.48}$	9.42
2-AP	$10.13_{0.52}$	$9.52_{0.01}$,[18] 9.40

improved treatment of this species would lead to better agreement with the experimental pK_8 values.

4.6. Speciation. Our species concentrations were calculated using the Henry Law based chemical potential model of eq 2, using our pK_1 and pK_2 values in conjunction with the well-known experimental pK data for reactions R3−R5.[81] We first calculated compositions using the ideal solution form of the model ($\ln \gamma_i = 0$) and then performed preliminary calculations using the methodology of Smith and Qi[49] for extending the model to the nonideal case. We found that the equilibrium compositions resulting from the first iteration of this approach changed by very small amounts from those of the ideal solution, and our results presented here are those of the ideal solution form of the model.

Whereas there exists extensive CO_2 solubility data as a function of its partial pressure for a wide range of amines, only a few NMR-based studies have studied speciation data in the solvent.[71,74,90,91] For the amines considered in this work, we only found NMR measurements for MEA and for AMP, which are shown in Figure 3 along with our predictions.

For MEA (left panel of Figure 3), our results are in excellent agreement with the experimental results at CO_2 loadings of 0.4 and greater, where the mole fractions are greater than about 0.005. There is significant scatter in the experimental data at low loadings for the HCO_3^-/CO_2^{-2} pair, reflecting the experimental difficulty of accurately measuring such low concentrations. As already noted in Section 4.4, these difficulties can lead to significant scatter in the experimentally determined pK_2 value if such data are used for its estimation.

Jakobsen et al.[90] fitted a thermodynamic model to their NMR data to separate the HCO_3^-/CO_2^{-2} and considered low CO_2 loadings. Our results are in better agreement with their data

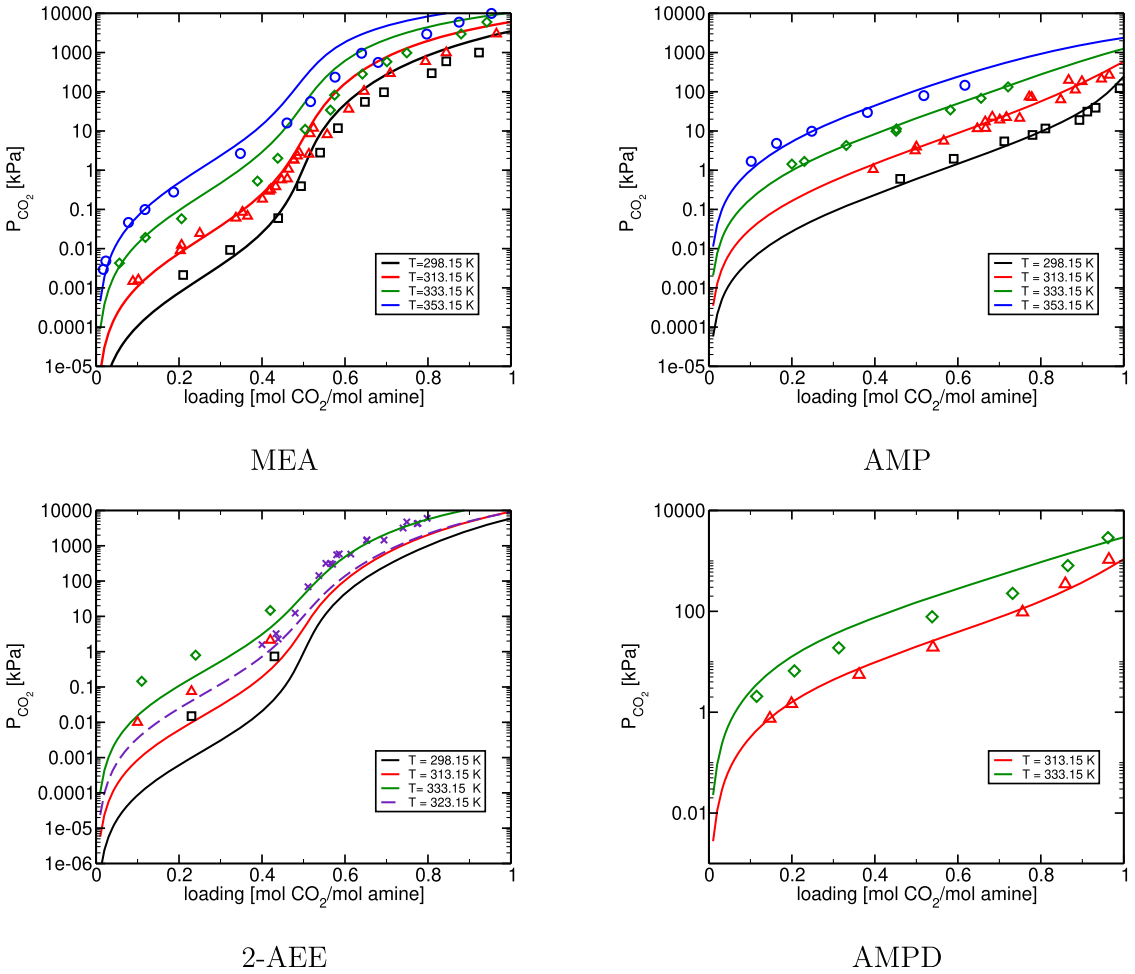

Figure 5. Comparison of the CO_2 partial pressures in 30 weight% MEA, AMP, AMPD and 60% 2-AEE aqueous solutions using the Henry Law based ideal-solution model at different temperatures with experimental data.[78,92−95] In the case of 2-AEE, stars indicate the experimental data of Martin et al.[93] and the other symbols are data of Al-Juaied et al.[78](65 wt % 2-AEE).

https://dx.doi.org/10.1021/acs.iecr.0c03738
Ind. Eng. Chem. Res. XXXX, XXX, XXX−XXX

(open blue circles) than those of Hilliard[91] (filled blue circles), which appear to under-predict the HCO_3^-/CO_3^{-2} concentrations. The inset shows that the Jakobsen et al.[90] HCO_3^- concentrations (open circles) agree well with our results, but their CO_3^{-2} concentrations are higher than ours (although both are quite small) at high loadings. This is consistent with the suggestion of the Jakobsen group that their +NMR speciation data did not obey electroneutrality, which they attributed to possible over-estimation of the CO_3^{-2} concentration. At higher loadings, our HCO_3^-/CO_3^{-2} results are in excellent agreement with the data of both Böttinger et al.[71] and Jakobsen et al.[90]

Finally, our results for the MEA carbamate species are in excellent agreement with those of Böttinger et al.[71] (filled squares), Jakobsen et al.[90] (open circles), and Hilliard (filled circles) at loadings up to about 0.6. At higher loadings, our predictions are in agreement with the data of Böttinger et al., who used a combination of ^{13}C and ^{1}H NMR procedures with the goal of obtaining more accurate carbamate concentrations. The Jakobsen et al. data are significantly higher.

In contrast to MEA, which is a carbamate forming species, AMP is a sterically hindered amine and forms only very small amounts of carbamate due to the electronic effect of the methyl groups around the nitrogen. As shown in the right panel of Figure 3, this is well captured by our simulations. Our predicted concentration of the HCO_3^-/CO_3^{-2} pair is in agreement with the Ciftja et al. measurements, whereas the AMP carbamate concentrations are significantly higher. The disagreement of $AMPCO_2^-$ concentration with the experimental NMR-based data of Ciftja et al.[74] can be justified in part by the fact that these concentrations are very small and that the speciation fraction data reported by Ciftja et al. do not obey electroneutrality, resulting in the likelihood that the carbamate concentrations are subject to significant uncertainties.

Finally, Figure 4 shows our predicted compositions for the other alkanolamines studied, for which no experimental data exist in the literature. If and when NMR experiments are performed for these solvents, we expect that species concentrations lower than about 0.005 will be either difficult to obtain accurately or undetectable. For example, for AMPD this is expected to be the case for the carbamate species, which will make the experimental determination of its pK_2 value very difficult.

4.7. CO_2 Solubility. The equilibrium solubility of CO_2 is expressed in terms of its partial pressure, P_{CO_2}, in the vapor phase as a function of the total loading (both in its free and chemically bound solution forms) in the solution phase. It is determined from the equality of the chemical potentials of its free solution form and in the vapor phase in reaction R6. At the relatively low total pressures typically involved, the vapor phase may be treated as an ideal gas, which yields the following equation for the P_{CO_2}:

$$P_{CO_2} = \left(\frac{RT}{100P^0}\right)\left(\frac{\bar{\rho}_{solv}(T,\tilde{P})}{1000}\right) m_{CO_2} \exp\left(\frac{\mu_{CO_2}^{res,NVT;\infty}(T,\rho(T,\tilde{P}))}{RT}\right) \quad (16)$$

The dependence of P_{CO_2} on loading at several temperatures considered is shown and compared with available experimental data in Figure 5 for 30 wt % MEA, AMP, AMPD and 60 wt % 2-(2-aminoethoxy)ethanol (2-AEE). For 2-AP shown in Figure 6, we only found a single solubility measurement at 313.15 K, with a CO_2 partial pressure of 15 kPa over 2 M (16 wt %) 2-AP aqueous solution.[96] It is seen that our predictions are in generally good agreement with the available experimental results.

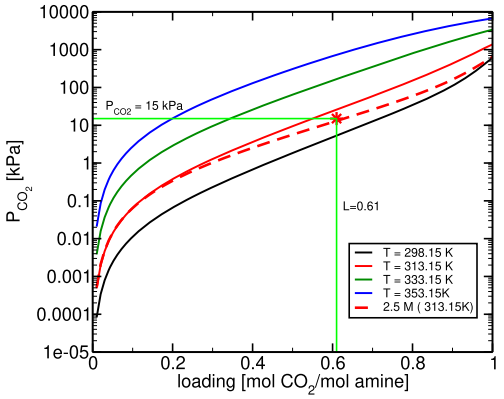

Figure 6. CO_2 solubility in 30 wt % (solid lines) and 16 wt % (dashed red line) 2-AP.

5. EFFECT OF AMINE CONCENTRATION ON CO_2 SOLUBILITY

Optimizing the amine concentration in the solvent is an important parameter for PCC system design. Our equilibrium model can be used to predict the effect of the amine concentration on the CO_2 solubility, and representative results are shown in Figure 7. It can be seen that, for the carbamate forming amines (MEA, 1-AP, SAPD), the amine concentration has a small effect on the CO_2 solubility for loadings below 0.5. At higher loadings, amine solutions of lower concentration will have a higher CO_2 solubility, attributed to the change from carbamate formation to bicarbonate formation. This "salting out" effect is more pronounced for MEA, which is a strong carbamate forming species, whereas it is less pronounced for SAPD, which we found to be a mild carbamate forming molecule. Similar to MEA, 1-AP is a carbamate forming amine, and the concentration is predicted to have a small effect on the CO_2 solubility at low loadings, in qualitative accordance with the trend of the scattered experimental data points in that loading range.

6. UNCERTAINTY ANALYSIS

Consideration of the effects of uncertainties in input model parameters on its outputs is a generally important aspect of modeling.[99−103] Experimental studies often use regression models to determine fundamental thermodynamic parameters such as the pK quantities shown in Table 1. These studies do not always provide uncertainty estimates for the pK values, but when they are provided, it is in the context of a particular combination of experimental and modeling approaches. A more reasonable indication of the uncertainty of experimentally determined pK values is the variation in the values obtained by different experimental groups using their different methodologies. In Section 4.2, we provided uncertainty estimates for our predictions.

Uncertainty analysis in the context of a nonlinear regression model of CO_2 reactive absorption has recently been considered

https://dx.doi.org/10.1021/acs.iecr.0c03738
Ind. Eng. Chem. Res. XXXX, XXX, XXX−XXX

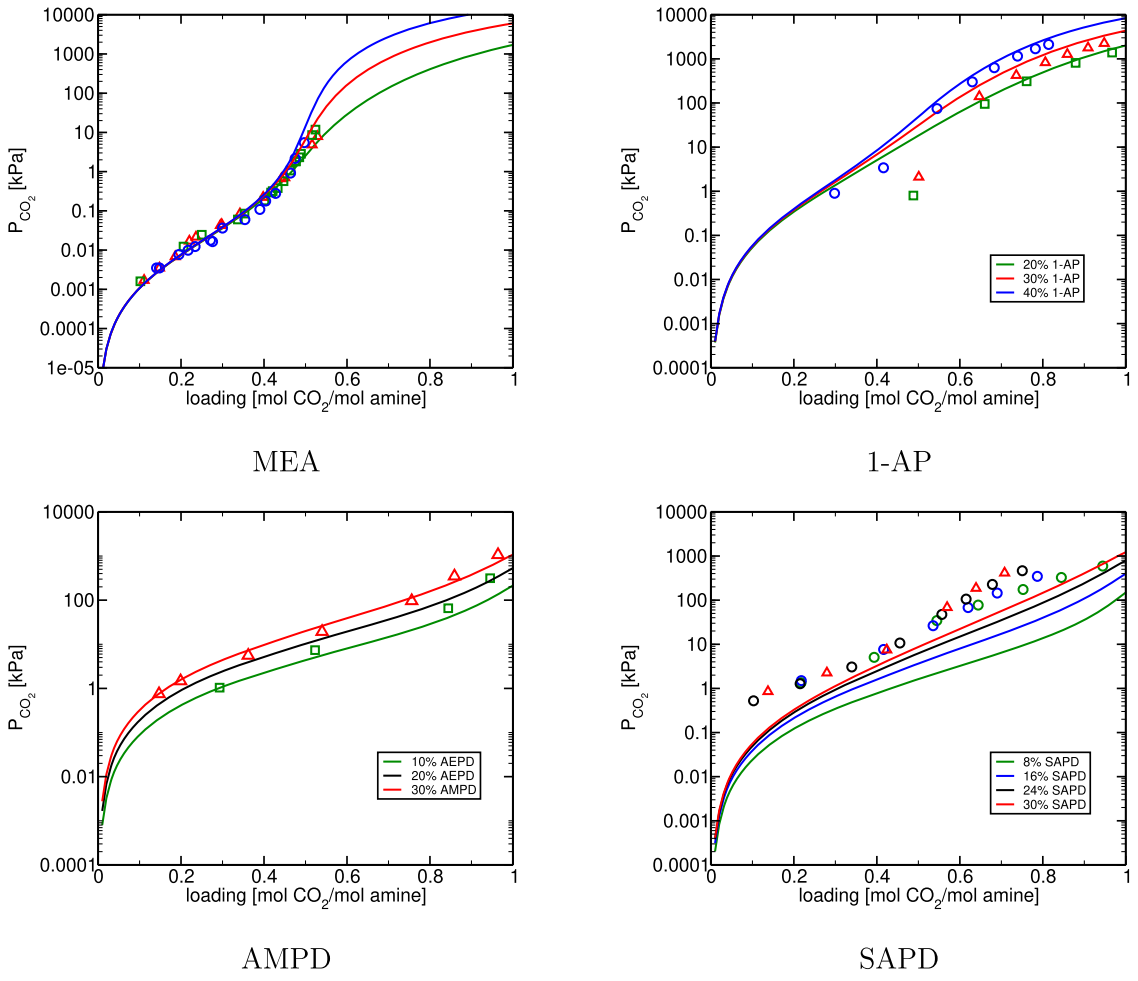

Figure 7. Effect of amine concentration on the CO_2 solubility of (a) MEA, (b) 1-AP, (c) AMPD, and (d) SAPD at 313.15 K, in comparison with experimental data.[80,94,97,98]

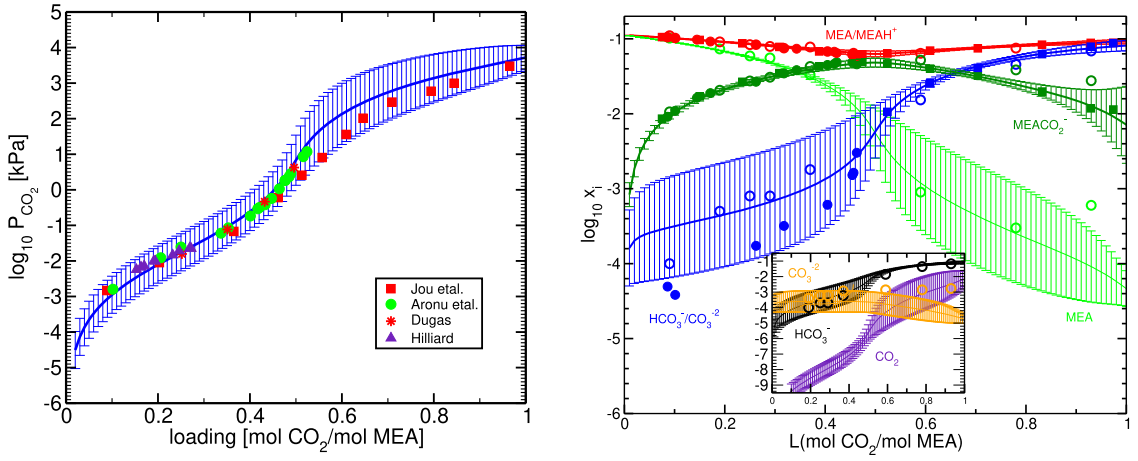

Figure 8. Left panel shows predicted values of P_{CO_2} in 30 wt % MEA at 313.15 K and their uncertainty intervals corresponding to one standard deviation, and comparison with experimental data.[91,92,97,104] The right panel shows the predicted solution concentrations and their one standard deviation uncertainty intervals for CO_2 in 30 with % MEA at 298.15 K, and comparison with the experimental data of Figure 3.

by Morgan et al.[102,103] by propagating the regressed model parameter uncertainties through the model to its P_{CO_2} output value. Using a previous version of the molecular-based predictive methodology of this paper, our earlier MEA study[44] provided uncertainty estimates for both P_{CO_2} and the solution compositions by propagating the pK uncertainties to these output quantities. Although the latter are important quantities, we are unaware of any other uncertainty study involving them.

The primary quantities used in our methodology to predict P_{CO_2} and speciation concentrations are the pK_1 and pK_2 values resulting from the ideal-gas free energy changes ΔG^0 and the species hydration free energies $\mu_i^{\mathrm{res},NVT;\infty}(T; P)$ in eqs 9−12.

https://dx.doi.org/10.1021/acs.iecr.0c03738
Ind. Eng. Chem. Res. XXXX, XXX, XXX−XXX

We calculated uncertainty estimates by an empirical bootstrapping procedure by generating 1000 sets of (pK_1, pK_2) values from independent normal distributions with means and variances given by the values in Table 1, and for each set we solved eq 1 for the resulting solution equilibrium compositions and P_{CO_2} as functions of the CO_2 loading. We then calculated the means and standard deviations of these compositions and P_{CO_2} values and expressed our uncertainties as one standard deviation of the predicted results.

Figure 8 shows representative results for the uncertainties of our predictions for P_{CO_2} for MEA at 313.15 K (left panel) and for the MEA solution compositions (right panel) at 298.15 K. We found no multiple sets of experimental P_{CO_2} and solution compositions at any common set of conditions, but we believe that the slight variations in the experimental temperatures do not significantly affect the results shown in the figures. The figures indicate that our predictions, and their precisions are compatible with the scatter of the experimental data. In the course of this study, w also found that pK_1 is the most important parameter at low loadings and that pK_2 is the most important at loadings greater than 0.5, for both P_{CO_2} and the solution species concentrations. We conclude from these figures that our predictive approach for the calculation of P_{CO_2} and the corresponding CO_2-loaded solution concentrations provides results of similar quality to those determined experimentally.

7. SUMMARY AND CONCLUSIONS

We have developed a purely predictive methodology that requires no experimental data of any kind for the amine solvent for predicting P_{CO_2} and the corresponding CO_2-loaded solution concentrations for the reactive absorption of CO_2 in a range of primary alkanolamine solvents. Our methodology is able to predict species concentrations of arbitrarily small magnitude, which are either difficult to measure or inaccessible experimentally. Since the reaction scheme is irrelevant for calculating equilibrium thermodynamic properties, ours was chosen to avoid the use of H^+ as a species, which is notoriously difficult to treat theoretically, due to the requirement to know the value of the hydration free energy of the proton as a function of temperature, an experimentally and theoretically elusive quantity. We applied our methodology to seven alkanolamine solvents and obtained excellent agreement with experimental results in cases when they are available, and made predictions in cases which have not yet been obtained.

Our algorithm entails the combination of the ideal-gas reaction standard free energies for the two reactions R1 and R2 using quantum mechanical methodology, and the calculation of hydration free energies for the solution species using classical force field methodology and standard molecular dynamics simulations. These quantities are appropriately translated to a macroscopically base thermodynamic model, from which P_{CO_2} and the solution concentrations are calculated by a free energy minimization algorithm.

We also calculated uncertainties for our predicted values of the relevant equilibrium constants, and for P_{CO_2} and the CO_2 loaded solution concentrations, by propagating the uncertainties in the ideal-gas quantities and hydration free energies through the equilibrium calculations to the final predicted quantities. We compared our predictions and their uncertainties with the corresponding experimental results obtained by different research groups (when these were available) and inferred the experimental uncertainties from the scatter of the data. For all quantities (with the possible slight exception of the value of pK_1), we conclude that our methodology provides predictions in mutual agreement with those obtained experimentally within their mutual uncertainties.

Potential improvements to our approach, which may be required for more complex solvents, would entail more accurate and precise estimates of the ideal-gas reaction free energies and of the species hydration free energies. The recently developed (on-the-fly polarization) OTFP methodology for calculating hydration free energies is one possibilty.[105,106] In addition, for more complex solutions it may be necessary to account for the nonideal activity coefficient behavior in the Henry Law based chemical potential model used in this paper. Although we have found this to be unnecessary for the solutions arising in the systems considered here, these may be incorporated by means of the ideal solution chemical potential extrapolation methodology of Smith and Qi.[49]

We suggest that our algorithm provides a potentially cost-effective screening methodology for improved solvent selection, and current work is underway to apply it to other potential solvents and their mixtures.

■ ASSOCIATED CONTENT

Supporting Information

The Supporting Information is available free of charge at https://pubs.acs.org/doi/10.1021/acs.iecr.0c03738.

Ideal-gas standard reaction free energies for reactions R1 and R2, fitted equilibrium constant expressions for R1 and R2, species $\mu^{res,NVT;\infty}$ values at several temperatures, values of quantities contributing to the equilibrium constants of reactions R1 and R2, and raw Gaussian16 output for the neutral, protonated and carbamate forms of the alkanolamines studied, and for the small molecules (PDF)

Gromacs topology and G4 geometry (ZIP)

■ AUTHOR INFORMATION

Corresponding Authors

Javad Noroozi − *Department of Chemical Engineering, University of Waterloo, Waterloo, ON N2L 3G1, Canada;* orcid.org/0000-0001-9718-4296; Email: jnoroozi@uwaterloo.ca

William R. Smith − *Department of Mathematics and Statistics, University of Guelph, Guelph, ON N1G 2W1, Canada; Department of Chemical Engineering, University of Waterloo, Waterloo, ON N2L 3G1, Canada; Faculty of Science, University of Ontario Institute of Technology, Oshawa, ON L1H 7K4, Canada;* orcid.org/0000-0002-1982-2050; Email: bilsmith@uoguelph.ca

Complete contact information is available at: https://pubs.acs.org/10.1021/acs.iecr.0c03738

Notes

The authors declare no competing financial interest.

■ ACKNOWLEDGMENTS

Financial support was provided by the Natural Science and Engineering Council of Canada (NSERC) and the Agence Nationale de la Recherche (ANR) through the International Collaborative Strategic program between Canada and France (Grant NSERC STPGP 479466-15 and ANR-12-IS09-0001-01). We thank our industrial partner, Dr. John Carroll, Gas

https://dx.doi.org/10.1021/acs.iecr.0c03738
Ind. Eng. Chem. Res. XXXX, XXX, XXX−XXX

Liquids Engineering Ltd., for supporting this research and for helpful advice and encouragement. Computational facilities of the SHARCNET (Shared Hierarchical Academic Research Computing Network) HPC consortium (www.sharcnet.ca) and Compute Canada (www.computecanada.ca) are gratefully acknowledged.

REFERENCES

(1) Kumoro, A. C.; Raksajati, A.; Ho, M.; Wiley, D.; Hadiyanto; Roces, S. A.; Yung, L.; Rong, X.; Lothongkum, A. W.; Phong, M. T.; Hussain, M. A.; Daud, W. R. W.; Nam, P. T. S. Solvent Development for Post-Combustion CO_2 Capture: Recent Development and Opportunities. *MATEC Web Conf.* **2018**, *156*, 03015.

(2) Song, C.; Liu, Q.; Ji, N.; Deng, S.; Zhao, J.; Li, Y.; Song, Y.; Li, H. Alternative pathways for efficient CO_2 capture by hybrid processes-A review. *Renewable Sustainable Energy Rev.* **2018**, *82*, 215−231.

(3) Dutcher, B.; Fan, M.; Russell, A. G. Amine−based CO_2 capture technology development from the beginning of 2013: A Review. *ACS Appl. Mater. Interfaces* **2015**, *7*, 2137−2148.

(4) Hartono, A.; Vevelstad, S. J.; Ciftja, A.; Knuutila, H. K. Screening of strong bicarbonate forming solvents for CO_2 capture. *Int. J. Greenhouse Gas Control* **2017**, *58*, 201−211.

(5) Barzagli, F.; Mani, F.; Peruzzini, M. Efficient CO_2 absorption and low temperature desorption with non-aqueous solvents based on 2-amino-2-methyl-1-propanol (AMP). *Int. J. Greenhouse Gas Control* **2013**, *16*, 217−223.

(6) Zhang, J.; Qiao, Y.; Agar, D. W. Improvement of lipophilic-amine-based thermomorphic biphasic solvent for energy-efficient carbon capture. *Energy Procedia* **2012**, *23*, 92−101.

(7) Pinto, D. D.; Zaidy, S. A.; Hartono, A.; Svendsen, H. F. Evaluation of a phase change solvent for CO_2 capture: Absorption and desorption tests. *Int. J. Greenhouse Gas Control* **2014**, *28*, 318−327.

(8) Choi, Y.-S.; Im, J.; Jeong, J. K.; Hong, S. Y.; Jang, H. G.; Cheong, M.; Lee, J. S.; Kim, H. S. CO_2 absorption and desorption in an aqueous solution of heavily hindered alkanolamine: Structural elucidation of CO_2−containing species. *Environ. Sci. Technol.* **2014**, *48*, 4163−4170.

(9) Smith, W. R.; Missen, R. W. *Chemical Reaction Equilibrium Analysis: Theory and Algorithms*; Krieger Publishing Co.; Reprint of same title, Willey-Interscience, 1982; Malabar, FL, 1991.

(10) Mahmud, N.; Benamor, A.; Nasser, M. S.; Tontiwachwuthikul, P. Carbamate Formation and Amine Protonation Constants in 2-Amino-1-Butanol−CO_2−H_2O System and Their Temperature Dependences. *J. Solution Chem.* **2018**, *47*, 262−277.

(11) Kamps, A. P.-S.; Maurer, G. Dissociation Constant of N-Methyldiethanolamine in Aqueous Solution at Temperatures from 278 to 368 K. *J. Chem. Eng. Data* **1996**, *41*, 1505−1513.

(12) Rayer, A. V.; Sumon, K. Z.; Jaffari, L.; Henni, A. Dissociation Constants (pKa) of Tertiary and Cyclic Amines: Structural and Temperature Dependences. *J. Chem. Eng. Data* **2014**, *59*, 3805−3813.

(13) Tagiuri, A.; Mohamedali, M.; Henni, A. Dissociation Constant (pKa) and Thermodynamic Properties of Some Tertiary and Cyclic Amines from (298 to 333) K. *J. Chem. Eng. Data* **2016**, *61*, 247−254.

(14) Ma'mun, S.; Kamariah; Sukirman; Kurniawan, D.; Amelia, E.; Rahmat, V.; Alwani, D. R.; Ismadji, S.; Agustina, T. E.; Yani, I.; Komariah, L. N.; Hasyim, S. Experimental determination of monoethanolamine protonation constant and its temperature dependency. *MATEC Web Conf.* **2017**, *101*, 02001.

(15) Bernhardsen, I. M.; Krokvik, I. R. T.; Perinu, C.; Pinto, D. D. D.; Jens, K. J.; Knuutila, H. K. Influence of pKa on solvent performance of MAPA promoted tertiary amines. *Int. J. Greenhouse Gas Control* **2018**, *68*, 68−76.

(16) Nguyen, W. H. C. H.; Henni, A. Dissociation Constant (pKa) and Thermodynamic Properties of 1,4-Bis(3-aminopropyl) Piperazine, 1,3-Bis(aminomethyl) Cyclohexane, Tris(2-aminoethyl) Amine, and 1-Amino-4-methyl Piperazine: Study of the Protonation Mechanism Using the Density Function Theory. *J. Chem. Eng. Data* **2020**, *65*, 2280.

(17) McCann, N.; Phan, D.; Fernandes, D.; Maeder, M. A systematic investigation of carbamate stability constants by ^1H NMR. *Int. J. Greenhouse Gas Control* **2011**, *5*, 396−400.

(18) Fernandes, D.; Conway, W.; Burns, R.; Lawrance, G.; Maeder, M.; Puxty, G. Investigations of primary and secondary amine carbamate stability by 1H NMR spectroscopy for post combustion capture of carbon dioxide. *J. Chem. Thermodyn.* **2012**, *54*, 183−191.

(19) Richner, G.; Puxty, G. Assessing the Chemical Speciation during CO_2 Absorption by Aqueous Amines Using in Situ FTIR. *Ind. Eng. Chem. Res.* **2012**, *51*, 14317−14324.

(20) McGregor, C.; Al-Abdul-Wahid, M. S.; Robertson, V.; Cox, J. S.; Tremaine, P. R. Formation Constants and Conformational Analysis of Carbamates in Aqueous Solutions of 2-Methylpiperidine and CO_2 from 283 to 313 K by NMR Spectroscopy. *J. Phys. Chem. B* **2018**, *122*, 9178−9190.

(21) Na, S.; Hwang, S. J.; Kim, H.; Baek, I.-H.; Lee, K. S. Modeling of CO_2 solubility of an aqueous polyamine solvent for CO_2 capture. *Chem. Eng. Sci.* **2019**, *204*, 140−150.

(22) Deshmukh, R. D.; Mather, A. E. A Mathematical Model for Equilibrium Solubility of Hydrogen Sulfide and Carbon Dioxide in Aqueous Alkanolamine Solutions. *Chem. Eng. Sci.* **1981**, *36*, 355−362.

(23) Najafloo, A.; Feyzi, F.; Zoghi, A. T. Modeling solubility of CO_2 in aqueous MDEA solution using electrolyte SAFT-HR EoS. *J. Taiwan Inst. Chem. Eng.* **2016**, *58*, 381−390.

(24) Lloret, J. O.; Vega, L. F.; Llovell, F. A Consistent and Transferable Thermodynamic Model to Accurately Describe CO_2 Capture with Monoethanolamine. *J. CO_2 Utilization* **2017**, *21*, 521−533.

(25) Pereira, L. M. C.; Vega, L. F. A systematic approach for the thermodynamic modelling of CO_2-amine absorption process using molecular-based models. *Appl. Energy* **2018**, *232*, 273−291.

(26) Wangler, A.; Sieder, G.; Ingram, T.; Heilig, M.; Held, C. Prediction of CO 2 and H 2 S solubility and enthalpy of absorption in reacting N-methyldiethanolamine /water systems with ePC-SAFT. *Fluid Phase Equilib.* **2018**, *461*, 15−27.

(27) Wang, T.; El Ahmar, E.; Coquelet, C.; Kontogeorgis, G. M. Improvement of the PR-CPA equation of state for modelling of acid gases solubilities in aqueous alkanolamine solutions. *Fluid Phase Equilib.* **2018**, *471*, 74−87.

(28) Wang, T.; Guittard, P.; Coquelet, C.; El Ahmar, E.; Baudouin, O.; Kontogeorgis, G. M. Improvement of the PR-CPA equation of state for modelling of acid gases solubilities in aqueous alkanolamine solutions. *Fluid Phase Equilib.* **2019**, *485*, 126−127.

(29) Klamt, A. The COSMO and COSMO-RS solvation models. *Wiley Interdiscip. Rev.: Comput. Mol. Sci.* **2011**, *1*, 699−709.

(30) Gerlach, T.; Müller, S.; Smirnova, I. Development of a COSMO-RS based model for the calculation of phase equilibria in electrolyte systems. *AIChE J.* **2018**, *64*, 272−285.

(31) Marenich, A. V.; Cramer, C. J.; Truhlar, D. G. Universal solvation model based on solute electron density and on a continuum model of the solvent defined by the bulk dielectric constant and atomic surface tensions. *J. Phys. Chem. B* **2009**, *113*, 6378−6396.

(32) Gangarapu, S.; Marcelis, A. T.; Zuilhof, H. Carbamate stabilities of sterically hindered amines from quantum chemical methods: Relevance for CO_2 capture. *ChemPhysChem* **2013**, *14*, 3936−3943.

(33) Xie, H.-B.; He, N.; Song, Z.; Chen, J.; Li, X. Theoretical investigation on the different reaction mechanisms of aqueous 2-amino-2-methyl-1-propanol and monoethanolamine with CO_2. *Ind. Eng. Chem. Res.* **2014**, *53*, 3363−3372.

(34) Gerlach, T.; Ingram, T.; Sieder, G.; Smirnova, I. Modeling the solubility of CO_2 in aqueous methyl diethanolamine solutions with an electrolyte model based on COSMO-RS. *Fluid Phase Equilib.* **2018**, *461*, 39−50.

(35) Gupta, M.; Svendsen, H. F. Modeling temperature dependent and absolute carbamate stability constants of amines for CO_2 capture. *Int. J. Greenhouse Gas Control* **2020**, *98*, 103061.

(36) Teranishi, K.; Ishikawa, A.; Sato, H.; Nakai, H. Systematic Investigation of the Thermodynamic Properties of Amine Solvents for

https://dx.doi.org/10.1021/acs.iecr.0c03738
Ind. Eng. Chem. Res. XXXX, XXX, XXX−XXX

CO_2 Chemical Absorption Using the Cluster-Continuum Model. *Bull. Chem. Soc. Jpn.* **2017**, *90*, 451−460.
(37) Haworth, N. L.; Wang, Q.; Coote, M. L. Modeling flexible molecules in solution: A pKa Case Study. *J. Phys. Chem. A* **2017**, *121*, 5217−5225.
(38) Nakai, H.; Nishimura, Y.; Kaiho, T.; Kubota, T.; Sato, H. Contrasting mechanisms for CO_2 absorption and regeneration processes in aqueous amine solutions: Insights from density-functional tight-binding molecular dynamics simulations. *Chem. Phys. Lett.* **2016**, *647*, 127−131.
(39) Sakti, A. W.; Nishimura, Y.; Nakai, H. Rigorous pKa Estimation of Amine Species Using Density-Functional Tight-Binding-Based Metadynamics Simulations. *J. Chem. Theory Comput.* **2018**, *14*, 351−356.
(40) Sakti, A. W.; Nishimura, Y.; Sato, H.; Nakai, H. Divide-and-Conquer Density-Functional Tight-Binding Molecular Dynamics Study on the Formation of Carbamate Ions during CO_2 Chemical Absorption in Aqueous Amine Solution. *Bull. Chem. Soc. Jpn.* **2017**, *90*, 1230−1235.
(41) Fetisov, E. O.; Kuo, I.-F. W.; Knight, C.; VandeVondele, J.; Van Voorhis, T.; Siepmann, J. I. First-Principles Monte Carlo simulations of reaction equilibria in compressed vapors. *ACS Cent. Sci.* **2016**, *2*, 409−415.
(42) Balaji, S. P.; Gangarapu, S.; Ramdin, M.; Torres-Knoop, A.; Zuilhof, H.; Goetheer, E. L.; Dubbeldam, D.; Vlugt, T. J. Simulating the Reactions of CO_2 in Aqueous Monoethanolamine Solution by Reaction Ensemble Monte Carlo Using the Continuous Fractional Component Method. *J. Chem. Theory Comput.* **2015**, *11*, 2661−2669.
(43) Mullen, R. G.; Corcelli, S. A.; Maginn, E. J. Reaction Ensemble Monte Carlo Simulations of CO_2 Absorption in the Reactive Ionic Liquid Triethyl(octyl)phosphonium 2-Cyanopyrrolide. *J. Phys. Chem. Lett.* **2018**, *9*, 5213.
(44) Noroozi, J.; Smith, W. R. An efficient molecular simulation methodology for chemical reaction equilibria in electrolyte solutions: Application to CO_2 reactive absorption. *J. Phys. Chem. A* **2019**, *123*, 4074−4086.
(45) Noroozi, J.; Smith, W. R. Prediction of Alkanolamine pK_a Values by Combined Molecular Dynamics Free Energy Simulations and ab Initio Calculations. *J. Chem. Eng. Data* **2020**, *65*, 1358.
(46) Smith, W. R.; Tríska, B. The Reaction Ensemble Method for the Computer Simulation of Chemical and Phase Equilibria. I. Theory and Basic Examples. *J. Chem. Phys.* **1994**, *100*, 3019−3027.
(47) Turner, C. H.; Brennan, J. K.; Lísal, M.; Smith, W. R.; Karl Johnson, J.; Gubbins, K. E. Simulation of Chemical Reaction Equilibria by the Reaction Ensemble Monte Carlo Method: A Review. *Mol. Simul.* **2008**, *34*, 119−146.
(48) Johnson, K. J.; Panagiotopoulos, Z. A.; Gubbins, K. E. A New Simulation Technique for Reacting or Associating Fluids. *Mol. Phys.* **1994**, *81*, 717−733.
(49) Smith, W. R.; Qi, W. Molecular Simulation of Chemical Reaction Equilibrium by Computationally Efficient Free Energy Minimization. *ACS Cent. Sci.* **2018**, *4*, 1185−1193.
(50) Nezbeda, I.; Moučka, F.; Smith, W. R. Recent progress in molecular simulation of aqueous electrolytes: force fields, chemical potentials and solubility. *Mol. Phys.* **2016**, *114*, 1665−1690.
(51) McQuarrie, D. A. *Statistical Mechanics*; University Science Books: Sausalito, CA, 2000.
(52) Ochterski, J. W. Thermochemistry in Gaussian. *Gaussian Inc* **2000**, *1*, 19.
(53) *Spartan18*; Wavefunction Inc.: 2018, Irvine, CA.
(54) Frisch, M. J. et al. *Gaussian 09*, revision E.01; Gaussian Inc.: Wallingford, CT, 2009.
(55) Wang, J.; Wolf, R. M.; Caldwell, J. W.; Kollman, P. A.; Case, D. A. Development and Testing of a General Amber Force Field. *J. Comput. Chem.* **2004**, *25*, 1157−1174.
(56) Wang, J.; Wang, W.; Kollman, P. A.; Case, D. A. Automatic atom type and bond type perception in molecular mechanical calculations. *J. Mol. Graphics Modell.* **2006**, *25*, 247−260.
(57) Potoff, J. J.; Siepmann, J. I. Vapor-Liquid Equilibria of Mixtures Containing Alkanes, Carbon Dioxide, and Nitrogen. *AIChE J.* **2001**, *47*, 1676−1682.
(58) Bayly, C. I.; Cieplak, P.; Cornell, W.; Kollman, P. A. A well-behaved electrostatic potential based method using charge restraints for deriving atomic charges: the RESP model. *J. Phys. Chem.* **1993**, *97*, 10269−10280.
(59) da Silva, A. W. S.; Vranken, W. F. ACPYPE-Antechamber python parser interface. *BMC Res. Notes* **2012**, *5*, 367.
(60) Pronk, S.; Pall, S.; Schulz, R.; Larsson, P.; Bjelkmar, P.; Apostolov, R.; Shirts, M. R.; Smith, J. C.; Kasson, P. M.; van der Spoel, D.; Hess, B.; Lindahl, E. GROMACS 4.5: a high−throughput and highly parallel open source molecular simulation toolkit. *Bioinformatics* **2013**, *29*, 845−854.
(61) Martinez, L.; Andrade, R.; Birgin, E. G.; Martinez, J. M. PACKMOL: a package for building initial configurations for molecular dynamics simulations. *J. Comput. Chem.* **2009**, *30*, 2157−2164.
(62) Beutler, T. C.; Mark, A. E.; van Schaik, R. C.; Gerber, P. R.; Van Gunsteren, W. F. Avoiding singularities and numerical instabilities in free energy calculations based on molecular simulations. *Chem. Phys. Lett.* **1994**, *222*, 529−539.
(63) Simmie, J. M.; Somers, K. P. Benchmarking compound methods (CBS-QB3, CBS-APNO, G3, G4, W1BD) against the active thermochemical tables: a litmus test for cost-effective molecular formation enthalpies. *J. Phys. Chem. A* **2015**, *119*, 7235−7246.
(64) Mobley, D. L.; Dumont, E.; Chodera, J. D.; Dill, K. A. Comparison of charge models for fixed-charge force fields: small-molecule hydration free energies in explicit solvent. *J. Phys. Chem. B* **2007**, *111*, 2242−2254.
(65) Jämbeck, J. P.; Mocci, F.; Lyubartsev, A. P.; Laaksonen, A. Partial atomic charges and their impact on the free energy of solvation. *J. Comput. Chem.* **2013**, *34*, 187−197.
(66) Kroutil, O.; Predota, M.; Kabelac, M. Force field parametrization of hydrogenoxalate and oxalate anions with scaled charges. *J. Mol. Model.* **2017**, *23*, 327.
(67) Jensen, M. B.; Jorgensen, E.; Faurholt, C. Reactions between carbon dioxide and amino alcohols. I. Monoethanoamine and Diethanolamine. *Acta Chem. Scand.* **1954**, *8*, 1137−1140.
(68) Austgen, D. M.; Rochelle, G. T.; Peng, X.; Chen, C. C. Model of Vapor Liquid Equilibria for Aqueous Acid Gas Alkanolamine Systems Using the Electrolyte NRTL Equation. *Ind. Eng. Chem. Res.* **1989**, *28*, 1060−1073.
(69) Aroua, M. K.; Benamor, A.; Haji-Sulaiman, M. Z. Equilibrium Constant for Carbamate Formation from Monoethanolamine and Its Relationship with Temperature. *J. Chem. Eng. Data* **1999**, *44*, 887−891.
(70) Conway, W.; Wang, X.; Fernandes, D.; Burns, R.; Lawrance, G.; Puxty, G.; Maeder, M. Comprehensive kinetic and thermodynamic study of the reactions of CO_2(aq) and HCO_3^- with monoethanolamine (MEA) in aqueous solution. *J. Phys. Chem. A* **2011**, *115*, 14340−9.
(71) Böttinger, W.; Maiwald, M.; Hasse, H. Online NMR spectroscopic study of species distribution in MEA−H_2O−CO_2 and DEA−H_2O−CO_2. *Fluid Phase Equilib.* **2008**, *263*, 131−143.
(72) Kim, I.; Hoff, K. A.; Hessen, E. T.; Haug-Warberg, T.; Svendsen, H. F. Enthalpy of absorption of CO_2 with alkanolamine solutions predicted from reaction equilibrium constants. *Chem. Eng. Sci.* **2009**, *64*, 2027−2038.
(73) McCann, N.; Maeder, M.; Hasse, H. A calorimetric study of carbamate formation. *J. Chem. Thermodyn.* **2011**, *43*, 664−669.
(74) Ciftja, A. F.; Hartono, A.; Svendsen, H. F. Experimental study on carbamate formation in the AMP−CO_2−H_2O system at different temperatures. *Chem. Eng. Sci.* **2014**, *107*, 317−327.
(75) Sartori, G.; Savage, D. W. Sterically hindered amines for carbon dioxide removal from gases. *Ind. Eng. Chem. Fundam.* **1983**, *22*, 239−249.
(76) Yamada, H.; Shimizu, S.; Okabe, H.; Matsuzaki, Y.; Chowdhury, F. A.; Fujioka, Y. Prediction of the basicity of aqueous amine solutions and the species distribution in the amine-H_2O-CO_2 system using the COSMO-RS method. *Ind. Eng. Chem. Res.* **2010**, *49*, 2449−2455.

https://dx.doi.org/10.1021/acs.iecr.0c03738
Ind. Eng. Chem. Res. XXXX, XXX, XXX−XXX

(77) Conway, W.; Wang, X.; Fernandes, D.; Burns, R.; Lawrance, G.; Puxty, G.; Maeder, M. Toward the understanding of chemical absorption processes for post-combustion capture of carbon dioxide: electronic and steric considerations from the kinetics of reactions of $CO_2$2 (aq) with sterically hindered amines. *Environ. Sci. Technol.* **2013**, *47*, 1163−1169.
(78) Al-Juaied, M.; Rochelle, G. T. Thermodynamics and equilibrium solubility of carbon dioxide in diglycolamine/morpholine/water. *J. Chem. Eng. Data* **2006**, *51*, 708−717.
(79) Ciftja, A. F.; Hartono, A.; da Silva, E. F.; Svendsen, H. F. Study on carbamate stability in the Amp/CO_2/H_2O system from 13C-NMR spectroscopy. *Energy Procedia* **2011**, *4*, 614−620.
(80) Bougie, F.; Iliuta, M. C. Solubility of CO_2 in and density, viscosity, and surface tension of aqueous 2-amino-1, 3-propanediol (serinol) solutions. *J. Chem. Eng. Data* **2014**, *59*, 355−361.
(81) Edwards, T.; Maurer, G.; Newman, J.; Prausnitz, J. Vapor-liquid equilibria in multicomponent aqueous solutions of volatile weak electrolytes. *AIChE J.* **1978**, *24*, 966−976.
(82) Liu, S.; Gao, H.; He, C.; Liang, Z. Experimental evaluation of highly efficient primary and secondary amines with lower energy by a novel method for post-combustion CO_2 capture. *Appl. Energy* **2019**, *233*−*234*, 443−452.
(83) Hamborg, E. S.; Versteeg, G. F. Dissociation Constants and Thermodynamic Properties of Amines and Alkanolamines from (293 to 353) K. *J. Chem. Eng. Data* **2009**, *54*, 1318−1328.
(84) Bates, R.; Pinching, G. D. Acidic Dissociation Constant and Related Thermodynamic Quantities for Monoethanolammonium Ion in Water From 0 to 500 C. *J. Res. Natl. Bur. Stand.* **1951**, *46*, 349−352.
(85) Kim, J.-H.; Dobrogowska, C.; Hepler, L. G. Thermodynamics of ionization of aqueous alkanolamines. *Can. J. Chem.* **1987**, *65*, 1726−1728.
(86) Antelo, J. M.; Arce, F.; Casado, J.; Sastre, M.; Varela, A. Protonation Constants of Mono-, Di-, and Triethanolamine. Influence of the Ionic Composition of the Medium. *J. Chem. Eng. Data* **1984**, *29*, 10−11.
(87) Datta, S. P.; Grzybowski, A. K. Acid Dissociation Constants of the Ammonium Group in 2-Aminoethanol, 2-Aminoethyl Phosphate, and 2-Aminoethyl Sulphate. *J. Chem. Soc.* **1962**, *568*, 3068−3077.
(88) Fernandes, D.; Conway, W.; Wang, X.; Burns, R.; Lawrance, G.; Maeder, M.; Puxty, G. Protonation constants and thermodynamic properties of amines for post combustion capture of CO_2. *J. Chem. Thermodyn.* **2012**, *51*, 97−102.
(89) Puxty, G.; Rowland, R.; Allport, A.; Yang, Q.; Bown, M.; Burns, R.; Maeder, M.; Attalla, M. Carbon Dioxide Postcombustion Capture: A Novel Screening Study of the Carbon Dioxide Absorption Performance of 76 Amines. *Environ. Sci. Technol.* **2009**, *43*, 6427−6433.
(90) Jakobsen, J. P.; Krane, J.; Svendsen, H. F. Liquid-phase composition determination in CO_2-H_2O-alkanolamine systems: An NMR study. *Ind. Eng. Chem. Res.* **2005**, *44*, 9894−9903.
(91) Hilliard, M. D. *A Predictive Thermodynamic Model for an Aqueous Blend of Potassium Carbonate, Piperazine, and Monoethanolamine for Carbon Dioxide Capture from Flue Gas*. Thesis, 2008.
(92) Jou, F.-Y.; Mather, A. E.; Otto, F. D. The solubility of CO_2 in a 30 mass percent monoethanolamine solution. *Can. J. Chem. Eng.* **1995**, *73*, 140−147.
(93) Martin, J. L.; Otto, F. D.; Mather, A. E. Solubility of hydrogen sulfide and carbon dioxide in a diglycolamine solution. *J. Chem. & Eng. Data 23*, 163−164.
(94) Baek, J.-I.; Yoon, J.-H. Solubility of carbon dioxide in aqueous solutions of 2-amino-2-methyl-1, 3-propanediol. *J. Chem. Eng. Data* **1998**, *43*, 635−637.
(95) Tong, D.; Trusler, J. M.; Maitland, G. C.; Gibbins, J.; Fennell, P. S. Solubility of carbon dioxide in aqueous solution of monoethanolamine or 2-amino-2-methyl-1-propanol: Experimental measurements and modelling. *Int. J. Greenhouse Gas Control* **2012**, *6*, 37−47.
(96) Liu, S.; Ling, H.; Gao, H.; Tontiwachwuthikul, P.; Liang, Z.; Zhang, H. Kinetics and new Brønsted correlations study of CO_2 absorption into primary and secondary alkanolamine with and without steric-hindrance. *Sep. Purif. Technol.* **2020**, *233*, 115998.
(97) Aronu, U. E.; Gondal, S.; Hessen, E. T.; Haug-Warberg, T.; Hartono, A.; Hoff, K. A.; Svendsen, H. F. Solubility of CO_2 in 15, 30, 45 and 60 mass from 40 to 120 °C and model representation using the extended UNIQUAC framework. *Chem. Eng. Sci.* **2012**, *78*, 246−247.
(98) Rebolledo-Morales, M. Á.; Rebolledo-Libreros, M. E.; Trejo, A. Equilibrium solubility of CO_2 in aqueous solutions of 1-amino-2-propanol as function of concentration, temperature, and pressure. *J. Chem. Thermodyn.* **2011**, *43*, 690−695.
(99) Smith, W. R.; Missen, R. W. Sensitivity analysis in ChE education. Part 1. Introduction and Application to explicit models. *Chem. Eng. Educ.* **2003**, *37*, 222−227.
(100) Smith, W. R.; Missen, R. W. Sensitivity Analysis in ChE Education. Part 2. Application to Implict Models. *Chem. Eng. Educ.* **2003**, *37*, 254−260.
(101) Mathias, P. M.; Gilmartin, J. P. Quantitative Evaluation of the Effect of Uncertainty in Property Models on the Simulated Performance of Solvent-Based CO_2-Capture. *Energy Procedia* **2014**, *63*, 1171−1185.
(102) Morgan, J. C.; Bhattacharyya, D.; Tong, C.; Miller, D. C. Uncertainty quantification of property models: Methodology and its application to CO_2-loaded aqueous MEA solutions. *AIChE J.* **2015**, *61*, 1822−1839.
(103) Morgan, J. C.; Chinen, A. S.; Omell, B.; Bhattacharyya, D.; Tong, C.; Miller, D. C. Thermodynamic modeling and uncertainty quantification of CO_2-loaded aqueous MEA solutions. *Chem. Eng. Sci.* **2017**, *168*, 309−324.
(104) Dugas, R. E.; Rochelle, G. T. CO_2 Absorption Rate into Concentrated Aqueous Monoethanolamine and Piperazine. *J. Chem. Eng. Data* **2011**, *56*, 2187.
(105) Kelly, B.; Smith, W. R. Alchemical hydration free-energy calculations using molecular dynamics with explicit polarization and induced polarity decoupling: an On-the-Fly polarization approach. *J. Chem. Theory Comput.* **2020**, *16*, 1146−1161.
(106) Kelly, B.; Smith, W. R. A Simple Method for Incorporating Polarization Effects in Solvation Free Energy Calculations Using Fixed-Charge Force Fields. *ACS Omega* **2020**, *5*, 17170.

https://dx.doi.org/10.1021/acs.iecr.0c03738
Ind. Eng. Chem. Res. XXXX, XXX, XXX−XXX